Applied Chemical Engineering (2026) Volume 9 Issue 1 ISSN: 2578-2010 (O)
doi: 10.59429/ace.v9i1.5854

ORIGINAL RESEARCH ARTICLE

Synthesis of Hydroxyapatite/Chitosan–Glutamic Acid Nanocomposite for Highly Efficient Removal of Congo Red Dye from Water

Huda Mahdi[1*], Saher Ali [1], Safa Ali [2]

[1] *Department of Chemistry, College of Science, University of Thi-Qar, Al-Nasyriah, Thi Qar, 64001, Iraq*

[2] *Department of Physics, College of Education, Al-Shatrah University, Al-Shatrah, Thi Qar, 64007, Iraq*

***Corresponding author:** Huda Mahdi; hud.mahdi@sci.utq.edu.iq

ABSTRACT

Water pollution by synthetic dyes from industrial effluents poses serious environmental and health risks. This study reports the synthesis, characterization, and application of a novel hydroxyapatite/chitosan-glutamic acid composite (HAP-Cs-Glu) for Congo red (CR) dye removal from aqueous solutions. The composite was synthesized via chemical precipitation at 80°C and pH 10 with 5 hours aging. Characterization was performed using XRD, FESEM, TEM, BET, and FTIR techniques. XRD confirmed hydroxyapatite formation with low crystallinity and 12.27 nm average crystal size. FESEM and TEM revealed spherical particles (~45.77 nm) composed of needle-like nanocrystals. BET analysis showed a surface area of 58.958 m^2/g, pore volume of 0.5538 cm^3/g, and average pore diameter of 37.572 nm. FTIR confirmed successful functionalization with characteristic phosphate, amino, and carboxyl bands. Batch adsorption experiments investigated effects of contact time (15-75 min), adsorbent dose (0.03-0.15 g), pH (3-9), initial concentration (200-600 mg/L), and temperature (313-333 K). Optimum conditions were: 600 mg/L CR concentration, pH 3, 0.03 g adsorbent, 45 min contact time, and 60°C, achieving maximum adsorption capacity of 833.33 mg/g. Kinetic data followed pseudo-second-order model (R^2 = 0.9996). Langmuir isotherm provided better fit than Freundlich, indicating monolayer adsorption. Thermodynamic analysis revealed spontaneous ($\Delta G° < 0$) and endothermic ($\Delta H° > 0$) adsorption with positive entropy change. The HAP-Cs-Glu composite demonstrates excellent potential as an eco-friendly adsorbent for CR removal from contaminated water.

Keywords: Hydroxyapatite, chitosan, glutamic acid, Congo red, adsorption, isotherm, thermodynamics

ARTICLE INFO

Received: 12 December 2025
Accepted: 22 January 2026
Available online: 30 January 2026

Graphical abstract

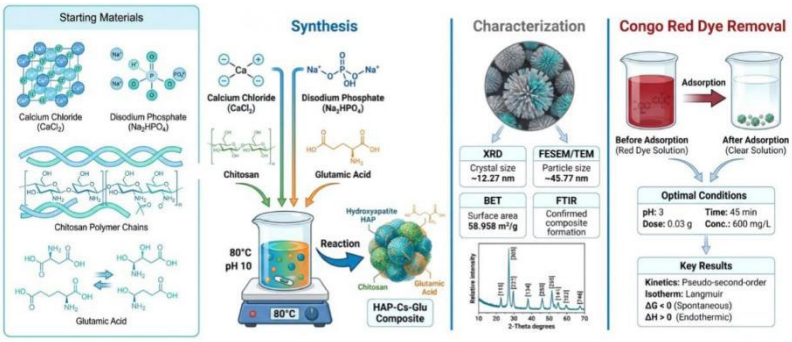

1. Introduction

The level of contaminants has increased over the past few decades as a result of industrial growth, and liquid waste containing pollutants like dyes has become a critical consequence for living creatures [1–3]. Over 10,000 species of commercial dyes and amounts of 7×10^5 tonnes are produced yearly [4,5], used in many industries, for example, textiles,

paper/pulp, polyamide fiber, dyeing wool, pharmaceuticals, cosmetics, leather, plastics, and food industries [6–8]. Congo red is an acidic azo dye that contains two –N=N– groups as chromophores and (–SO_3H) as acidic auxochromes, which link to benzene structures [9]. The complicated aromatic structure, thermal, optical, and physicochemical stability features of CR make it resistant to photo and biodegradation [10,11]. Those substances are poisonous because they involve aromatic rings, which cause cancer, allergies, mutations, and skin irritation [12,13]. Also, they affect aquatic ecosystems by banning sunlight from being permitted through water and affecting photosynthesis in plants, thereby causing serious aesthetic and environmental problems [14], leading to severe issues in aquatic ecosystems by shrinking the concentration of dissolved oxygen [15]. Therefore, treating these contaminants in the water is essential for organisms. There are many chemical, physical, and biological methods to deal with such pollutants such as chemical oxidation [16], photocatalytic degradation [17], coagulation–flocculation process [18], membrane filtration [19], precipitation [20], adsorption [21], and microbiological treatment [22] and stimuli-responsive nano hydrogels [23]. Among these various methods, adsorption has great interest because it is eco-friendly, simple, inexpensive, highly efficient, and the adsorbent can be reused [24]. Several studies have conveyed that various adsorbents such as fly ash [25], red mud [26], zeolite [27], activated carbon [28], leaf powder [29], and nanosilica [30] have been used to adsorb various azo dyes including Congo red. Recently, hydroxyapatite emerged as an adsorbent for eliminating long-term contaminants due to its efficiency, availability, non-toxicity, porous nature, stability, low cost, biocompatibility, and low water solubility [31]. Hydroxyapatite (HA) is an inorganic compound referred to calcium apatite, which is a member of the apatite family. The expression of apatite describes a group of compounds that have similar structures but not the same components [32,33]. HA has a certain composition, $Ca_5(PO_4)_3(OH)$, and is usually written as $Ca_{10}(PO_4)_6(OH)_2$ to show that the cell unit of hydroxyapatite crystal contains two entities [34,35]. Hydroxyapatite with low crystallinity has been synthesized by the precipitation method and used to improve the adsorption process and efficient removal of heavy metal ions from wastewater in the Rosia Montana mine [36]. The precipitation method combined with ultrasonication is an efficient procedure to prepare nano-hydroxyapatite (nHAP) and could be implemented as an environmental substance for soil remediation and wastewater treatment. The maximum adsorption capacity of nHAP to remove heavy metals such as copper, lead, cadmium, and zinc ions is 272, 1352, 304, and 285 mg/g respectively [37]. The adsorption performance of chitosan (Cs), which is a naturally abundant basic polymer produced from shrimp chitin, has improved through combination with nano-hydroxyapatite to eliminate cadmium ions from water. In contrast to pure Cs, the CS/n-HAP bio-composite demonstrated a higher capacity for Cd(II) adsorption under optimal conditions. The experimental maximum adsorption capacity reached 128.65 mg/g, which is roughly double that of pure Cs (67.5 mg/g) [38]. In a separate study, a hydroxyapatite/chitosan nanocomposite was applied for the removal of brilliant green (BG) dye from water [39]. The results showed the composite is an active adsorbent and the adsorption is endothermic and spontaneous. The adsorption capacity of chitosan-modified hydroxyapatite composite was greater than pure hydroxyapatite or pure chitosan, reaching 769 mg/g for removing Congo red from aqueous solution when the chitosan content was 50% [40]. On the other hand, nano-calcium apatite synthesized through the sol-gel method was a good adsorbent at ambient temperature to clean water from dyes such as Congo red. At optimal conditions, the adsorption capacity at equilibrium (qm) for CR of 100 ppm was found to be 487.80 mg/g. Moreover, thermodynamic calculations demonstrated that the adsorption was spontaneous, exothermic, and physisorption-based [41]. Although hydroxyapatite and chitosan have been extensively investigated individually and as binary composites for dye removal, the functionalization of hydroxyapatite with both chitosan and glutamic acid (HAP-Cs-Glu) for Congo red adsorption remains largely unexplored. The incorporation of glutamic acid introduces additional carboxyl and amino functional groups, which are expected to enhance the adsorption capacity through increased electrostatic interactions with anionic dye molecules. The HAP-Cs-Glu composite offers several advantages: (i) biocompatibility and non-toxicity inherited from all three components, (ii) enhanced surface functionality due to multiple active groups (hydroxyl, amino, carboxyl, and phosphate), (iii) improved adsorption capacity through synergistic effects, and (iv) eco-friendly nature

suitable for sustainable water treatment. In this study, HAP functionalized with chitosan–glutamic amino acid composite (HAP-Cs-Glu) will be prepared and utilized to remove Congo red dye pollutants from water. Also, many parameters that may affect adsorption will be investigated like contact time, pH, adsorbent dosage (HAP-Cs-Glu), initial concentration of adsorbate (Congo red), and temperature. Furthermore, Langmuir and Freundlich models will be studied using experimental data. The objectives of this study are: (1) to synthesize a novel HAP-Cs-Glu nanocomposite via chemical precipitation method; (2) to characterize the synthesized material using XRD, FESEM, TEM, BET, and FTIR techniques; (3) to evaluate the adsorption performance for Congo red removal under various experimental conditions; (4) to investigate the adsorption kinetics, isotherms, and thermodynamics; and (5) to assess the potential of HAP-Cs-Glu as an efficient adsorbent for industrial wastewater treatment.

2. Materials and methods

2.1. Materials

Calcium chloride, disodium phosphate, ammonium acetate, chitosan, L-glutamic acid, and Congo red dye were purchased from Hangzhou Hyper Chemicals Limited, Hangzhou, China. Ammonium hydroxide 32% and hydrochloric acid (35-38%) were obtained from Alpha chemika and sodium hydroxide from Fluka. All reagents were utilized without any additional purification. Deionized water is used to prepare all solutions.

2.2. Preparation of solid adsorbent

Hydroxyapatite functionalized by chitosan and glutamic amino acid particles (HAP-Cs-Glu) was synthesized by chemical precipitation according to the previous procedure [42] with some modifications. Briefly, 100 mL of 60 mM disodium phosphate Na_2HPO_4 was prepared in deionized water and added after adjusting the pH to 10 by ammonium hydroxide to 20 mL of 0.2 M of glutamic acid was prepared in 1.3 M of ammonium acetate CH_3COONH_4 solution at 80 °C, pH 10 drop by drop. Then 100 mL of 100 mM calcium chloride $CaCl_2$ was prepared in deionized water and mixed after adjusted pH=10 with 20 mL of 2% chitosan (dissolved in 1% acetic acid solution). The final solution after adjusted pH=10 added to the glutamic solution drop by drop. The precipitation (HAP-Cs-Glu) was aged at pH=10, temperature 80°C with continuous stirring for 5 h. The (HAP-Cs-Glu) particles were recaptured by centrifugation at speed (4,000 rpm) for 10 minutes and washed three times with deionized water and three times with ethyl alcohol. Finally, those particles were dried in an oven at 37°C for 24 hours until constant weight was achieved, then collected in a sealed container, and stored in a desiccator for further studies. This procedure was repeated to prepare pure hydroxyapatite.

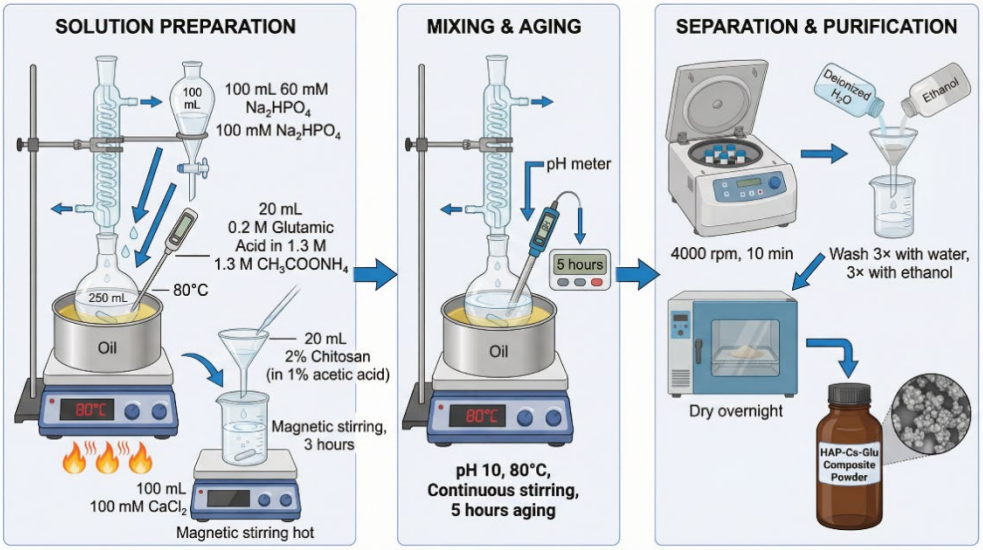

Figure 1. Schematic diagram of the HAP–Cs–Glu composite synthesis via chemical precipitation.

2.3. Characterization techniques

2.3.1. X-ray diffraction (XRD)

X-ray diffraction (PW1730 model, Phillips Company, Netherlands) was used to analyze the materials' crystal structure. Data were gathered using Cu Kα radiation (wave length=1.5406A˚) with a 2theta range of 10.28º to 79.98º at a step size of 0.05º. Debye Scherrer's equation was used to get the average crystal size (D_{hkl}) of the particles from the XRD model [43]:

$$D_{hkl} = 0.94\ \lambda/(\cos\theta_{hkl})(\beta_{hkl}) \quad (1)$$

Where k is constant and chosen to be 0.94 depending on the crystal nature, λ represents the wavelength of copper alpha radiation Cu Kα (1.54060 Å), β_{hkl} is the full width at the half maximum (FWHM) in radian and θ refers to the diffraction angle of plane hkl.

2.3.2. Electronic microscopy analysis (FESEM/TEM)

The samples' surface morphology and the average of particle′s size were examined with a (type Inspect F50, Fei company, Netherlands) field emission scanning electron microscope (FESEM). A Transmission Electron Microscope (TEM) (Zeiss-EM10C-100 KV model, Germany) was used to examine the microstructure of the produced composite.

2.3.3. Surface area estimation

The specific mean surface area of sample was found utilizing (BET) Brunauer, Emmett, and Teller instrument (BELSORP MINI II, BEL, Jaban) at 77K based on N_2 gas adsorption /desorption isotherms.

2.3.4. Fourier transform - infrared spectroscopy

The Bruker-Tensor 27 IR spectrometer was used to affirm the functionalization of HA with chitosan and amino acid (glutamic). Also, it is used to prove the adsorption of CR dye on the prepared composite surface.

2.4. Adsorption studies

All experiments have been carried out by dissolving Congo red (CR) in deionized water. In every procedure, the diluted fresh solution has been implemented. The adsorption procedures were conducted in 250 ml glass beakers with 50 ml of Congo red solutions mixed with an appropriate amount of adsorbent and agitated using a magnetic stirrer at a constant speed of 200 rpm. After reaching the adsorption equilibrium, the adsorbent was separated from the supernatant by using a centrifuge device (centrifuge 80-1, China) for 5min at 4000 rpm. The residue CR concentration was measured utilizing a T90+ UV-Visible spectrometer (PG Instruments Ltd) at a wavelength 499 nm. Data analysis and curve fitting were performed using OriginPro 2021 software (OriginLab Corporation, USA). Linear regression analysis was used to determine kinetic and isotherm parameters, with correlation coefficients (R^2) calculated to evaluate the goodness of fit. Some parameters that affect the CR adsorption process onto the (HAP-Cs-Glu) composite have been studied, such as contact time, amount of adsorbent, pH, temperature, and initial CR concentration. In the first study, the range of contact time was 15-75 minutes. The dose of the HAP-Cs-Glu varied in scope from 0.03-0.15g. The variation of temperature (T) was in the range of 40-60 ºC, while the initial CR concentration (C_o) was diversified in range (200-600) mg/L. The initial pH of CR solutions ranged from 3-9 was adjusting by a few drops of 0.1M NaOH or 0.1M HCl solutions. The removal efficiency of CR dye, and the adsorbed concentration at the equilibrium, q_e (mg/g) were calculated respectively. The percentage of dye removal and the quantity of adsorbed dye were calculated by the following mathematical expressions [44].

$$R_E\,\% = \left[\frac{C_o - Ce}{C_o}\right] \times 100 \quad (2)$$

$$qe = [V \times \frac{C_0 - Ce}{m}] \quad (3)$$

Where C_0 and C_e are the initial and residue concentrations of CR dye in solution (mg /L) at equilibrium respectively, V is the volume of dye solution (L), and m is the amount of HAP-Cs-Glu composite (g). After adsorption, the color of CR drastically decreased, indicating that the HAP-Cs-Glu particles fully adsorb it from the relevant solution (**Figure 2**). A few tests were conducted to assess the adsorption kinetics of CR.

Figure 2. Evidence of CR adsorption

3. Results and discussion

3.1. X-ray diffraction

The XRD pattern of the synthesized HAP-Cs-Glu composite is presented in **Figure 3**. The diffraction peaks observed at 2θ values of 25.51°, 31.55°, 39.41°, 49.45°, and 63.67° correspond to the (002), (211), (310), (213), and (502) crystallographic planes of hydroxyapatite, respectively. These peaks are in excellent agreement with the standard hydroxyapatite diffraction pattern (JCPDS Card No. 09-432), confirming the successful formation of the hydroxyapatite phase [45,46].

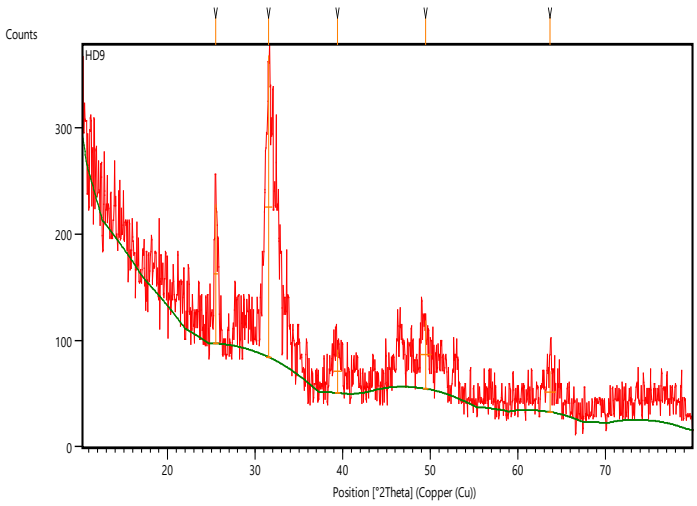

Figure 3. XRD for (HAP-Cs-Glu) composite

Because the powder is quite fine, the XRD style exhibits a significant degree of peak broadening [47]. Peak broadening may also be a signal that the substance contains nanosized crystals [48]. All of the peaks have low,

wide intensities, which suggests low crystallinity. Based on the Debye-Scherrer formula and the FWHM of the peaks, the average size of HAP-Cs-Glu crystals is around 12.27 nm.

3.2. Electronic microscopies (FESEM/TEM)

Electronic microscopies (FESEM/TEM) were used to examine the size and shape of the synthesized composite particles and the shape of the crystals. The results demonstrated that HAP-Cs-glu particles formed as spherical surfaces, and have a lot of grooves. The mean size of the particles was roughly 45.77nm, made up of needle-like nanocrystals as exhibited in **Figure 4**. The powder particles look strongly agglomerated in the FESEM micrographs, most likely due to their nanometric size [49]. Furthermore, the crosslinked long chain of Cs may have contributed to the HAp nanoparticles' apparent aggregation [50].

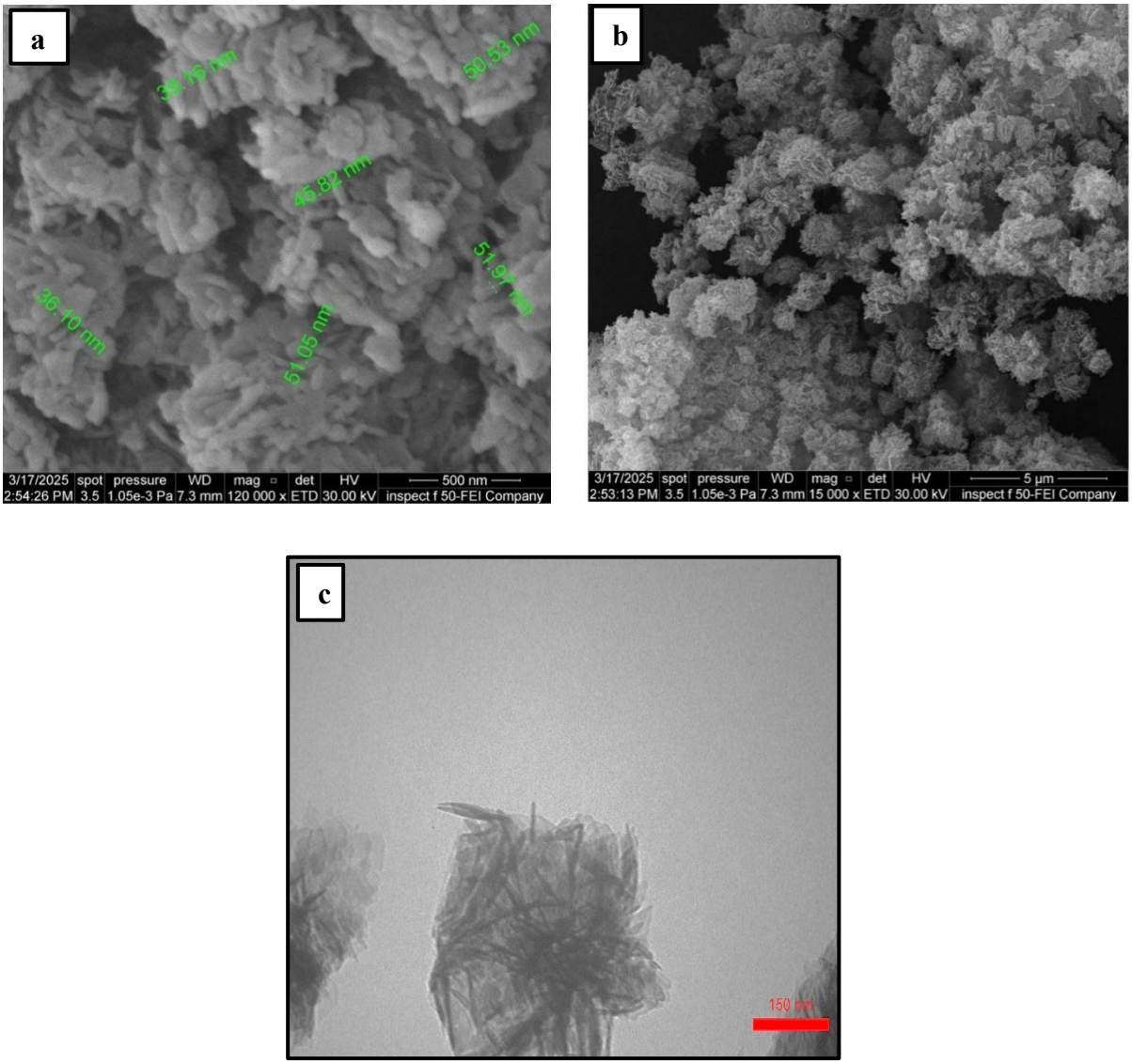

Figure 4. Electronic microscopy images of (HAP-Cs-Glu) composite a) FESEM at a scale 500 nm b) SEM at a scale 5 µm and c) TEM at a scale 150 nm

3.3. BET analysis

The N_2 adsorption-desorption assessments at a temperature of 77K for the synthesized composite were examined using the BET method. The calculated surface area (as), total pore volume and average pore diameter of the synthesized composite (HAP-Cs-Glu) were 58.958 m^2/g, 0.5538 cm^3/g, and 37.572 nm, respectively.

3.4. FT-IR analysis

The functional groups of prepared HA and HAP-Cs-Glu are illustrated in **Figure 5**. The sharp stretching band of HA at 3568 cm^{-1}, which seems to be a shoulder, belongs to the free OH stretch that may exist at the crystallite's surface[49]. A broad, strong peak -centered around 3424 cm^{-1} and a small broad peak at roughly 1645 can be attributed to the adsorbed H_2O on the HA surface[51]. Additionally, the strong, sharp bands of HA at 1032.87, 962.16, 603.70, 565.00, and 472.23 are assigned to the P-O bonds of PO_4^{-3} groups [52,53]. The last bands of HA (PO_4^{-3} bands) appear in the prepared composite with a shift to low wavelength. The strong and broad band that centered at 3446.02 cm^{-1} belongs to the OH and NH_2 from Cs [54], overlapping with the OH of adsorbed water and the structural OH of HA, while the band at 2925.65 cm^{-1} is due to the C-H streching. The broad band centered at 1640.33 cm^{-1} is assigned to the adsorbed water (OH bending vibration) overlapping with amide I (C=O) and amide II (NH) of Cs. Moreover, the strong two signals that are located at 1456.11 and 1421.24 cm^{-1} in composite due to symmetric vibration modes of $NH3^{+}$and COO^{-} respectively [42]. All mentioned above refer to the formation of the HAP-Cs-Glu composite successfully.

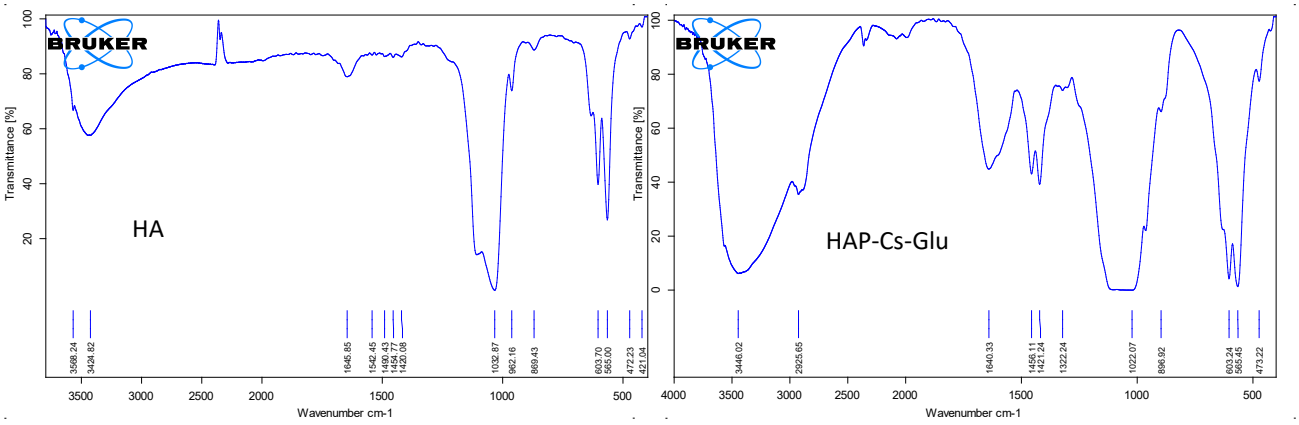

Figure 5. FT-IR for prepared HA and HAP-Cs-Glu.

3.5. Adsorption studies

3.5.1. Contact Time's effect and the adsorption kinetics

The effect of contact time on the CR adsorption on the HAP-Cs-Glu surface is displayed in **Figure 6**. It was found that as the contact period increased from (15-75) minutes, the adsorption of CR dye on the prepared composite increased considerably. It is clear that the elimination of CR started out quite quickly (within 30 minutes) and then slowed down till equilibrium. This behavior is due to the available active sites at the first stages, after 30 min, and when the process reaches a fixed stage, all the active sites will be occupied with CR [55]. In general, it was found that 45 minutes of contact time was enough to guarantee that this adsorbent hit saturation in its CR sorption capability.

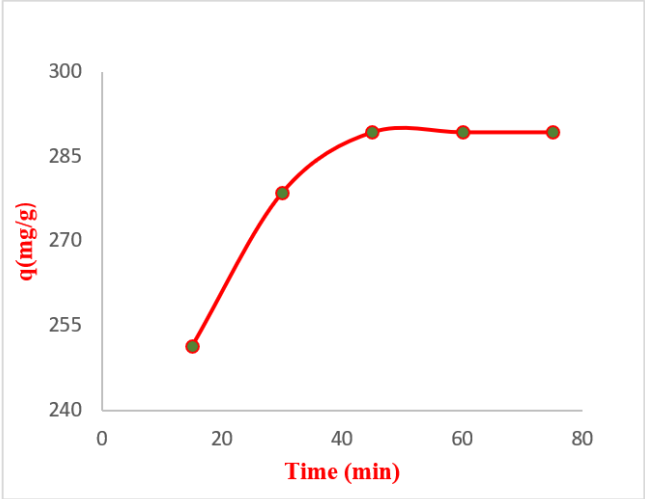

Figure 6. Effect of contact time on the CR adsorption capacity

The kinetics of CR adsorption on the (HAP-Cs-Glu) composite are displayed in **Figure 7**. Plotting t/qt versus t using the linear version of the pseudo-second-order kinetic model allowed for the investigation of the rate of CR adsorption. Equation (4) was used to evaluate the second-order constants (k and qe) for composite [56], which are mentioned in **Table 1**.

$$\frac{t}{q_t}=\frac{1}{k_2 q_e^2}+\frac{t}{q_e} \tag{4}$$

q_t and q_e refer to the quantities of CR adsorbed on HAP-Cs-Glu (mg/g) at time t and equilibrium, respectively. k_2 represents the rate constant (g/mg min) of the pseudo-second order adsorption kinetics.

Pseudo-second order kinetics are confirmed by a linear plot of t/qt vs. t, where the values of q_e and k_2 are calculated from the slope and the intercept respectively. Remarkably, the experimental results were perfectly fitted by the pseudo-second order kinetic model, where the estimated equilibrium sorption and the observed sorption closely matched.

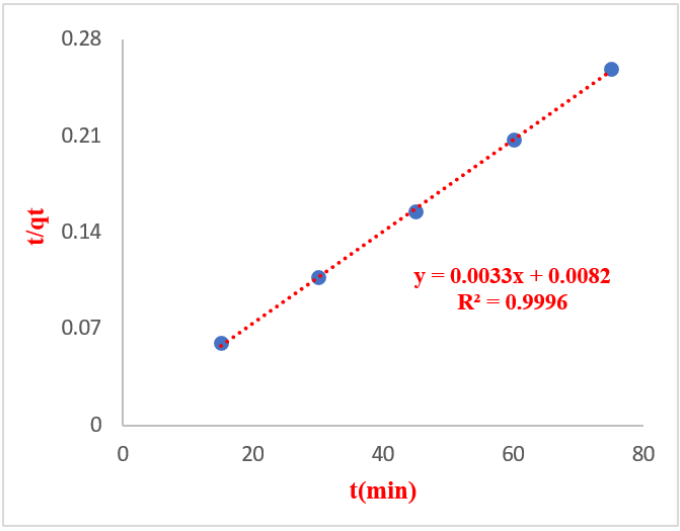

Figure 7. pseudo-second order kinetic model for CR adsorption on the surface of HAP-Cs-Glu (Co= 300 mg/L, adsorbent dose=0.05 g and natural pH).

Table 1. The parameters derived from applying the pseudo-second order equation (Eq. (4)) to fit the sorption data of CR onto (HAP-Cs-Glu) composite. R represents the linear plot's regression coefficient.

adsorbent	k_2 (g/mg min)	q_e (mg/g)	R^2

HAP-Cs-Glu	1.3280*10-3	303	0.9996

3.5.2. Adsorbent dosage's effect

In an effort to optimize the CR adsorption process using the HAP-Cs-Glu composite, **Figure 8** shows the results of an investigation on the impact of the HAP-Cs-Glu dose. As predictable, the CR adsorption % increased quickly (71.74 to 98.68%) with increasing the HAP-Cs-Glu dosage (0.03 to 0.15 g), due to expanding the number of adsorption sites accessible for the CR removal. Remarkably, a CR removal efficiency of 98.68% could be attained using 0.15 g of HAP-Cs-Glu. In contrast, the CR adsorption capacity to the HAP-Cs-Glu dose falls because adding more quantity of adsorbent results in reducing the unsaturation of adsorption locations, and then the number of these sites per unit mass goes down [57,58]. Therefore, the process should be customized to use the least quantity of HAP-Cs-Glu dose while achieving the best removal effectiveness for CR. As a consequence, the amount of 0.03g of composite was chosen for further studies.

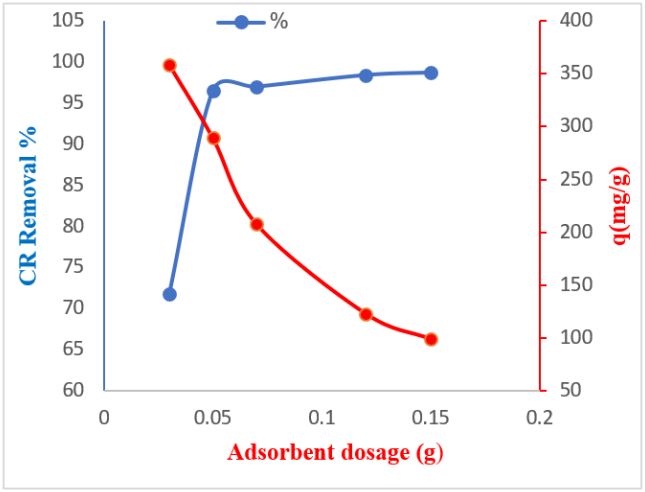

Figure 8. Effect of HAP-Cs-Glu dose on the CR removal (Co=300 mg/L, solution volume=50 ml, contact time = 45min, and natural pH)

3.5.3. The pH's effect

The pH range of 3 to 9 was used to investigate how pH affected the adsorption process of CR on HAP-Cs-Glu surface. As shown in **Figure 9**, the pH can affect the adsorption kinetics and adsorption capacity of dye on adsorbent solid surfaces by altering the surface charges of the adsorbent, and CR molecules present at various pH values [59]. The SO_3 groups of the CR dye (D-SO_3Na) dissociate and transform into anions in aqueous solution according to the following equation [60]:

$$D\text{-}SO_3Na \xrightarrow{H_2O} D\text{-}SO_3^- + Na_+ \quad (5)$$

Since, prepared composite contains amino groups (NH_2) in both chitosan and glutamic acid, which can be protonated in acidic medium by hydrogen ions (H^+) of the solution [61]

$$R'\text{-}NH_2 + H_+ \rightleftharpoons R'\text{-}NH_3^+ \quad (6)$$

Therefore, the composite surface is expected to hold positive charges. Thus, at low pH, there is a significantly strong electrostatic attractive between CR dye (negatively charged) and adsorbent's surface (positively charged) [62].

$$R'\text{-}NH_3^+ + DSO_3^- \rightleftharpoons R'\text{-}NH_3^+ \cdots O_3SD \quad (7)$$

On the other hand, the numbering of negatively charged positions rises and the numbering of positively charged positions falls as the system′s pH increases. The electrostatic repulsion between the negatively charged sites on the adsorbent surface and the dye anions may be one of the reasons for lower adsorption. Also, alkaline pH leads to an increase in the number of OH, which compete with CR anions for active sites on the adsorbent surface [63].

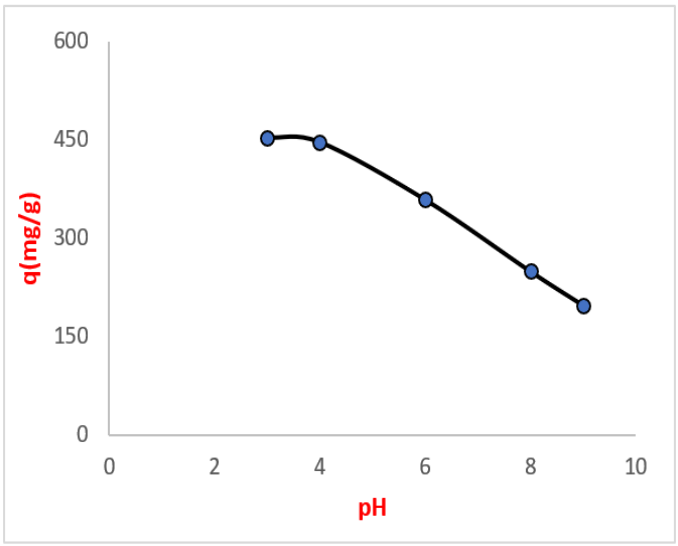

Figure 9. Effect of pH on the CR removal (Co=300 mg/L, adsorbent dose= 0.03g, contact time 45min)

3.5.4. The initial concentration′s effect

The effect of initial dye concentration on the adsorption process was studied, using different dye concentrations (200-600 ppm) with constant adsorbent weight. A gradual decrease in the removal percentage was observed, accompanied by an increase in the adsorption efficiency values with increasing dye concentration, as illustrated in **Figure 10**. This is because increasing the initial CR concentration causes the concentration gradient's driving force to increase [64].

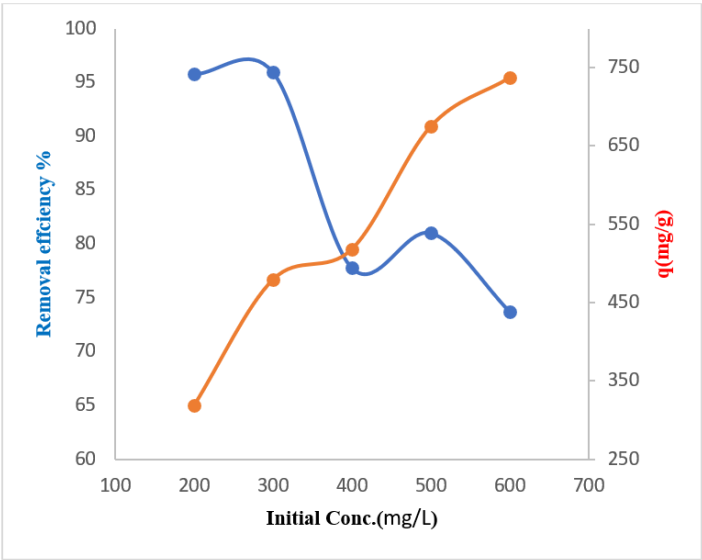

Figure 10. Effect of initial concentration of CR on adsorption capacity at (adsorbent dose = 0.03g, pH =3, contact time = 45 min, temperature=40°C).

The highest adsorption capacity (737.26 mg/g) was recorded at the highest concentration (600 mg/L). In contrast, the removal efficiency was 73.726% for the composite at the same concentration, as the inverse

relationship between the initial dye concentration and the removal efficiency. This behavior can be explained through only a small number of dye molecules can be adsorbed by the active sites of adsorbent at low initial dye concentrations. On the other hand, at high initial dye concentrations, the constant number of active sites on the adsorbents cannot remove an increasing number of dye molecules; as a result, the percentage of dye molecules that stay in the solution rises, reducing the removal of dye [65].

3.5.5. Effect of temperature

The adsorption of Congo red dye on the surface of (HAP-Cs-Glu) was studied at three temperatures (313, 323, and 333 K) and different concentrations (200-600 mg/L) with the weight of the adsorbent surface fixed (0.03 g) and the contact time (45 min) for the composite. It is noted from **Figure 11** that increasing the temperature is accompanied by increasing the adsorption capacity, which indicates that the adsorption process on the (HAP-Cs-Glu) surface is an endothermic process.

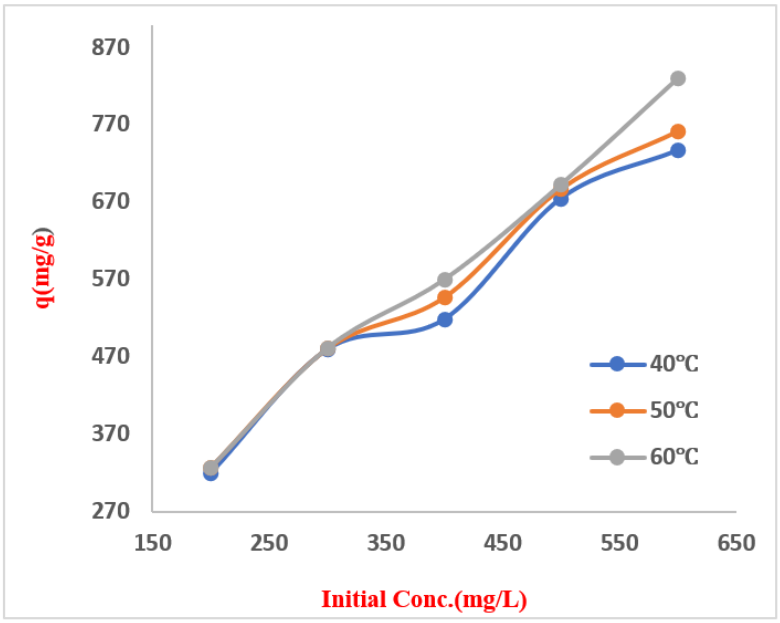

Figure 11. Effect of Temperature on adsorption capacity of CR at (adsorbent dose = 0.03g, pH =3, Contact time = 45 min).

3.5.6. Calculation of thermodynamic functions

In order to investigate the viability of the adsorption process, the following mathematical formulas (8-10) can be used to determine thermodynamic functions such as free energy (ΔG^o), enthalpy (ΔH^o), and entropy (ΔS^o) changes [66].

$$K=\frac{C_{Ae}}{C_e} \tag{8}$$

$$\Delta G°=-RTlnK \tag{9}$$

$$lnK=-\frac{\Delta H°}{RT}+\frac{\Delta S°}{R} \tag{10}$$

Where K is known as equilibrium constant, C_e and C_{Ae} refer to the residue CR concentration in solution and the adsorbed CR concentration on the HACs-Glu surface, respectively, R represents the universal gas constant, and its value is 8.314 kJ/mol. K, and T is the solution's absolute temperature in kelvin (K). The thermodynamic parameters ($\Delta H°$ and $\Delta S°$) can be obtained from the slopes and the intercepts of the Van't Hoff equation (10) by plotting lnK against 1/T, as clarified in **Figure 12**.

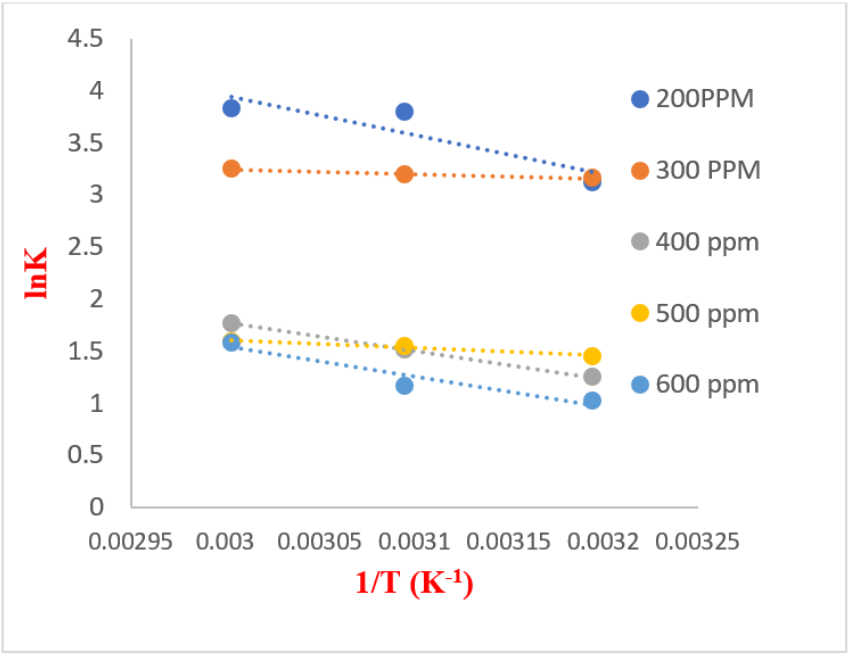

Figure 12. Estimation of thermodynamic functions from plotting lnK against 1/T for CR adsorption on the prepared composite

Table 2 displayed the thermodynamic parameters that were collected. The adsorption procedure is implied to be spontaneous by the negative ΔG values. At elevated temperatures, adsorption is more spontaneous, as seen by the drop in ΔG values with increasing temperature [67]. Positive values of entropy change and enthalpy change indicate that the adsorbed species' degree of freedom has increased, and an adsorption procedure is endothermic [68]. These results are consistent with those of earlier research [69].

Table 2. Thermodynamic functions for the CR adsorption onto the prepared composite surface.

Concentration of CR dye mg/L	ΔH^0 (kJ/mol)	ΔS^0 (J/K.mol)	ΔG^0 (kJ/ mol)			R^2
			T=313K	T=323K	T=333K	
200	31.599	127.7	-8.1166	-10.2172	-10.6239	0.8011
300	3.712	38.13	-8.2333	-8.5924	-8.9959	0.9869
400	22.6348	82.70	-3.2605	-4.0770	-4.9093	0.9999
500	6.4445	32.720	-3.7765	-4.1739	-4.4260	0.9585
600	24.143	85.276	-2.6849	-3.1338	-4.4024	0.9067

3.5.7. Adsorption isotherms

Adsorption isotherms depict the relevance between the amount of the adsorbed dye (mg) per adsorbent mass (g) and dye's concentration in the solution [70]. Langmuir and Freundlich isotherm models were utilized to describe the adsorption of a variety of adsorbate concentrations to evaluate adsorption isotherms and their capacity to correlate with experimental findings. Equation (11) of the Langmuir model assumes that a limited number of active binding sites are uniformly distributed across a particular adsorbent surface [71]. These binding sites possess the identical affinity to adsorb a monomolecular layer, and the adsorbed molecules do not interact with one another [72].

$$\frac{C_e}{q_e} = \frac{1}{K_L q_{max}} + \frac{C_e}{q_{max}} \qquad (11)$$

C_e represents the dyes' equilibrium concentration (mg/L), q_e is the quantity of dye adsorbed per certain quantity of adsorbent composite (mg/g), K_L is defined as Langmuir equilibrium constant (L/mg), and the theoretical maximum capacity of adsorption (mg/g) is denoted by q_{max}. When C_e/q_e is plotted versus C_e, as exhibited in **Figure 13** and the data undergoes linear regression. It is possible to compute the q_e and K_L constants using the slope and intercept.

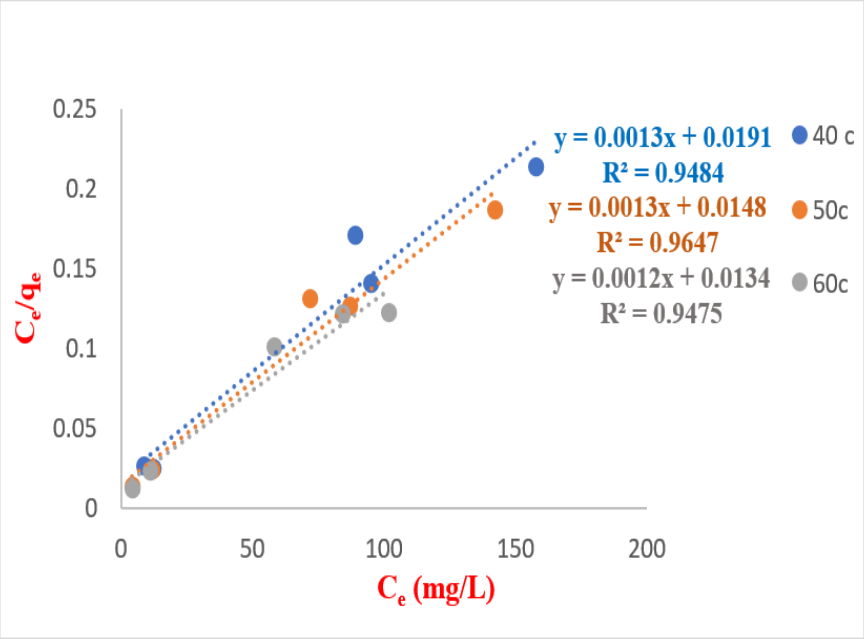

Figure 13. Langmuir isotherms for CR adsorption on HAP-Cs-Glu surface at various temperatures.

The key features of the Langmuir pattern can be described in expressions of the separation factor (R_L) [73] which is explained by

$$R_L = \frac{1}{1+K_L C_0} \tag{12}$$

The isotherm type is indicated by the R_L value, which can be either irreversible ($R_L = 0$), favorable ($0 < R_L < 1$), linear ($R_L = 1$) or unfavorable ($R_L > 1$) [74] . The R_L worth was determined to be 0.04-0.03 at different temperatures, and these ensure that the isotherm of Langmuir was favorable for CR adsorption onto (HAP-Cs-Glu) composite surface. **Table 3** lists the characteristics of the Langmuir isotherm for the CR adsorption onto the hydroxyapatite composite.

The Freundlich model, Eq. (13), is widely used to represent the adsorption properties of multilayer, heterogeneous surfaces and active centers are distributed exponentially [75]. The following is its linearized version [76].

$$lnq_e = \frac{1}{n} lnC_e + lnK_F \tag{13}$$

The Freundlich constant, which determines adsorption capacity, is represented as K_F, and the favorability constant for the adsorption process is denoted by 1/n. The adsorption procedure is favorable when $0 < n < 10$ [75]. The linear graph of lnq_e against lnC_e as shown in **Figure 14** is typically used to measure the values of n and K_F utilizing both the slope and intercept, respectively. **Table 3** lists the characteristics of the Freundlich isotherm for the CR adsorption onto hydroxyapatite composite. Langmuir isotherm approach was found to be better compared to Freundlich model when R^2 was examined against each other as shown in **Table 3**.

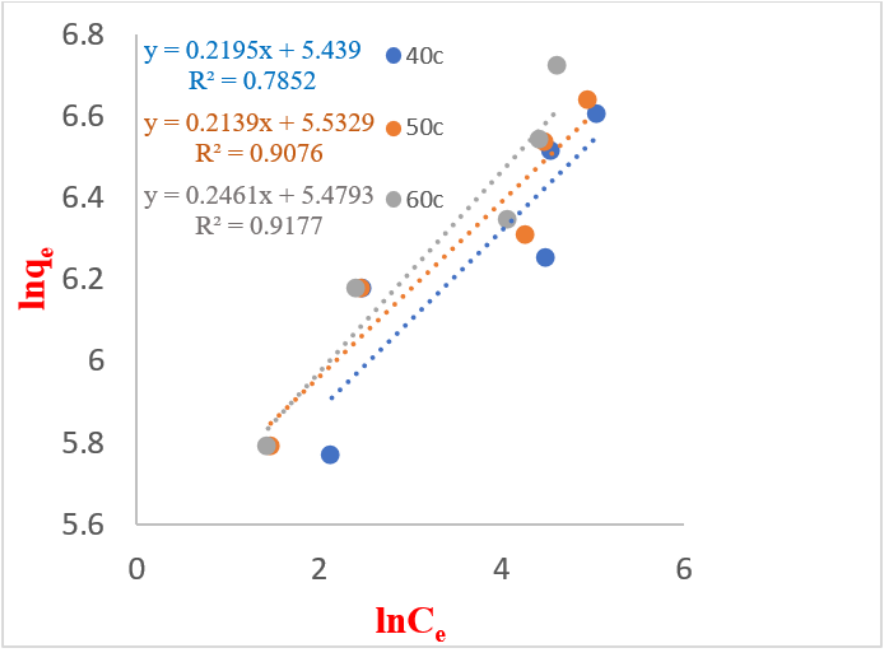

Figure 14. Freundlich isotherms for CR adsorption on HAP-Cs-Glu surface at various temperatures.

Table 3. CR adsorption isotherm constants on hydroxyapatite composite under different temperatures.

	Langmuir				Freundlich		
Temp (°C)	**q_{max}**	**K_L**	**R_L**	**R^2**	**K_F**	**n**	**R^2**
40	769.230	0.06806	0.04055	0.9484	230.211	4.5558	0.7852
50	769.230	0.08783	0.03179	0.9647	252.876	4.6750	0.9076
60	833.333	0.08955	0.03120	0.9475	239.678	4.0633	0.9177

As shown in **Table 4**, the HAP-Cs-Glu composite exhibits superior adsorption capacity compared to previously reported adsorbents, demonstrating the effectiveness of glutamic acid functionalization in enhancing Congo red removal.

Table 4. Comparison of CR adsorption capacity of HAP-Cs-Glu with other adsorbents

Adsorbent	**q_{max} (mg/g)**	**Reference**
HAP-Cs-Glu (this work)	833.33	Present study
Chitosan-modified HAP	769.00	[39]
Nano-calcium apatite	487.80	[40]
Nano silica	333.3	[29]
Fly-ash@ Fe_3O_4	153	[24]
Activated carbon	75.76	[27]

4. Conclusion

A novel HAP-Cs-Glu composite was successfully synthesized via chemical precipitation and demonstrated excellent performance for Congo red dye removal from aqueous solutions. Characterization confirmed the formation of nanocrystalline hydroxyapatite (12.27 nm crystal size) with spherical particle morphology (45.77 nm), high surface area (58.958 m^2/g), and successful functionalization with chitosan and glutamic acid. The adsorption process was highly pH-dependent, with maximum efficiency at pH 3 due to electrostatic attraction between protonated amino groups (NH_3^+) on the composite surface and anionic

sulfonate groups (SO3-) of CR molecules. Under optimum conditions (600 mg/L CR, pH 3, 0.03 g adsorbent, 45 min, 60°C), the composite achieved a remarkable maximum adsorption capacity of 833.33 mg/g. The adsorption kinetics followed the pseudo-second-order model ($R^2 = 0.9996$), suggesting chemisorption as the rate-controlling step, while equilibrium data fitted best to the Langmuir isotherm, indicating monolayer adsorption on a homogeneous surface. Thermodynamic parameters confirmed that the process was spontaneous ($\Delta G° < 0$), endothermic ($\Delta H° > 0$), and accompanied by increased randomness ($\Delta S° > 0$). These findings demonstrate that HAP-Cs-Glu composite is a highly effective, eco-friendly, and promising adsorbent for treating dye-contaminated industrial wastewater.

Conflict of interest

The authors declare no conflict of interest

References

1. Tahira, I.; Aslam, Z.; Abbas, A.; Monim-Ul-Mehboob, M.; Ali, S.; Asghar, A. Adsorptive removal of acidic dye onto grafted chitosan: A plausible grafting and adsorption mechanism. Int. J. Biol. Macromol. 2019, 136, 1209–1218. https://doi.org/10.1016/j.ijbiomac.2019.06.173.
2. Kim, H.; Park, C.; Choi, N.; Cho, K. Congo red dye degradation using Fe-containing mineral as a reactive material derived from waste foundry dust. Environ. Sci. Pollut. Res. 2024, 31 (19), 28443–28453. https://doi.org/10.1007/s11356-024-33064-9.
3. Ali, N. M. Removal of (Crystal Violet, Janus Green) dyes by poly acrylic acid hydrogel beads. Univ. Thi-Qar J. Sci. 2023, 10 (1), 48–54. https://doi.org/10.32792/utq/utjsci/v10i1.925.
4. Ali, S. A. K. Dye removal from wastewater. IJSRSET 2017, IJSRSET1731130, 3 (5). ISSN 2395-1990 (Print); 2394-4099 (Online).
5. Hernández-Zamora, M.; Martínez-Jerónimo, F. Congo red dye diversely affects organisms of different trophic levels: A comparative study with microalgae, cladocerans, and zebrafish embryos. Environ. Sci. Pollut. Res. 2019, 26 (12), 11743–11755. https://doi.org/10.1007/s11356-019-04589-1.
6. Majeed, H. A. S. A. Synthesis, characterization, and study of the spectral and electronic properties of a new azo dyes compounds. J. Thi-Qar Sci. 2013, 4 (1). ISSN 1991-8690.
7. Farooq, M.; Ramli, A.; Naeem, A.; Shah, L. A.; Mahmood, T.; Tariq, M.; Khan, J.; Perveen, F.; Humayun, M. Photocatalytic degradation of Acid Yellow 17 azo dye using ZrO2–CeO2 hollow macrospheres as a catalyst. Desalin. Water Treat. 2019, 170, 318–324. https://doi.org/10.5004/dwt.2019.24685.
8. Obaid, H. T. Study the effect of changing positions on some of the spectral properties of the new azo dye [sodium (E)-7-amino-3-((2-(hydrogenarsonato)phenyl)diazenyl)-3-hydroxynaphthalene-1-sulfonate] and compare it with other azo dye prepared in advance [sodium (Z)-4-amino-2-((2-(hydrogenarsonato)phenyl)diazenyl)-4-hydroxynaphthalene-2-sulfonate]. J. Thi-Qar Sci. 2017, 6 (2). ISSN 1991-8690.
9. Siddiqui, S. I.; Allehyani, E. S.; Al-Harbi, S. A.; Hasan, Z.; Abomuti, M. A.; Rajor, H. K.; Oh, S. Investigation of Congo Red toxicity towards different living organisms: A review. Processes 2023, 11 (3), 807. https://doi.org/10.3390/pr11030807.
10. Rao, T. M.; Rao, V. V. B. Biosorption of Congo Red from aqueous solution by crab shell residue: A comprehensive study. SpringerPlus 2016, 5 (1). https://doi.org/10.1186/s40064-016-2113-9.
11. Chatterjee, S.; Lee, D. S.; Lee, M. W.; Woo, S. H. Congo red adsorption from aqueous solutions by using chitosan hydrogel beads impregnated with nonionic or anionic surfactant. Bioresour. Technol. 2009, 100 (17), 3862–3868. https://doi.org/10.1016/j.biortech.2009.03.023.
12. Sivarajasekar, N.; Baskar, R. Adsorption of basic red 9 on activated waste Gossypium hirsutum seeds: Process modeling, analysis and optimization using statistical design. J. Ind. Eng. Chem. 2013, 20 (5), 2699–2709. https://doi.org/10.1016/j.jiec.2013.10.058.
13. Velkova, Z. Y.; Kirova, G. K.; Stoytcheva, M. S.; Gochev, V. Biosorption of Congo Red and Methylene Blue by pretreated waste Streptomyces fradiae biomass—Equilibrium, kinetic and thermodynamic studies. J. Serb. Chem. Soc. 2017, 83 (1), 107–120. https://doi.org/10.2298/jsc170519093v.
14. Rani, K. C.; Naik, A.; Chaurasiya, R. S.; Raghavarao, K. S. M. S. Removal of toxic Congo red dye from water employing low-cost coconut residual fiber. Water Sci. Technol. 2017, 75 (9), 2225–2236. https://doi.org/10.2166/wst.2017.109.
15. Adly, E. R.; Shaban, M. S.; El-Sherbeeny, A. M.; Zoubi, W. A.; Abukhadra, M. R. Enhanced Congo Red adsorption and photo-Fenton oxidation over an iron-impeded geopolymer from ferruginous kaolinite: Steric, energetic, oxidation, and synergetic studies. ACS Omega 2022, 7 (35), 31218–31232. https://doi.org/10.1021/acsomega.2c03365.

16. Zouboulis, A.; Zamboulis, D.; Szymanska, K. Hybrid membrane processes for the treatment of surface water and mitigation of membrane fouling. Sep. Purif. Technol. 2014, 137, 43–52. https://doi.org/10.1016/j.seppur.2014.09.023.
17. Fowsiya, J.; Madhumitha, G.; Al-Dhabi, N. A.; Arasu, M. V. Photocatalytic degradation of Congo red using Carissa edulis extract capped zinc oxide nanoparticles. J. Photochem. Photobiol. B 2016, 162, 395–401. https://doi.org/10.1016/j.jphotobiol.2016.07.011.
18. Kristianto, H.; Rahman, H.; Prasetyo, S.; Sugih, A. K. Removal of Congo red aqueous solution using Leucaena leucocephala seed's extract as natural coagulant. Appl. Water Sci. 2019, 9 (4). https://doi.org/10.1007/s13201-019-0972-2.
19. Rambabu, K.; Bharath, G.; Monash, P.; Velu, S.; Banat, F.; Naushad, M.; Arthanareeswaran, G.; Show, P. L. Effective treatment of dye polluted wastewater using nanoporous CaCl2 modified polyethersulfone membrane. Process Saf. Environ. Prot. 2019, 124, 266–278. https://doi.org/10.1016/j.psep.2019.02.015.
20. Alotaibi, N. F.; Nassar, A. M.; Alrwaili, G. M.; Elnasr, T. A. S.; Zeid, E. F. A. Selective, efficient and complete precipitation of anionic dyes in aqueous solutions using Ag@PbCO3 nanocomposite. Inorg. Nano-Met. Chem. 2019, 49 (11), 395–400. https://doi.org/10.1080/24701556.2019.1661463.
21. Nodehi, R.; Shayesteh, H.; Kelishami, A. R. Enhanced adsorption of congo red using cationic surfactant functionalized zeolite particles. Microchem. J. 2019, 153, 104281. https://doi.org/10.1016/j.microc.2019.104281.
22. Silva, E. R.; Dall'Oglio, E. L.; Vasconcelos, L. G.; Morais, E. B. Decolorization of the benzidine-based azo dye Congo red by the new strain Shewanella xiamenensis G5-03. Braz. J. Biol. 2021, 82. https://doi.org/10.1590/1519-6984.237386.
23. Thamer, A.N.; Turki, H.J.; Hassan, A.H.; Jasim, L.S.; Haider, M.N. Stimuli-Responsive Nano Hydrogels for Sustainable Water Pollution Reduction: A Comprehensive Review of Design, Performance, and Industrial Translation. Journal of Nanostructures 2026, 16 (1), 568-584. https://doi.org/10.22052/JNS.2026.01.051
24. Karimi, H.; Ghaedi, M. Application of artificial neural network and genetic algorithm to modeling and optimization of removal of methylene blue using activated carbon. J. Ind. Eng. Chem. 2013, 20 (4), 2471–2476. https://doi.org/10.1016/j.jiec.2013.10.028.
25. Harja, M.; Lupu, N.; Chiriac, H.; Herea, D.; Buema, G. Studies on the removal of congo red dye by an adsorbent based on Fly-Ash@Fe3O4 mixture. Magnetochemistry 2022, 8 (10), 125. https://doi.org/10.3390/magnetochemistry8100125.
26. Tor, A.; Cengeloglu, Y. Removal of congo red from aqueous solution by adsorption onto acid activated red mud. J. Hazard. Mater. 2006, 138 (2), 409–415. https://doi.org/10.1016/j.jhazmat.2006.04.063.
27. Imessaoudene, A.; Cheikh, S.; Hadadi, A.; Hamri, N.; Bollinger, J.; Amrane, A.; Tahraoui, H.; Manseri, A.; Mouni, L. Adsorption performance of zeolite for the removal of Congo red dye: Factorial design experiments, kinetic, and equilibrium studies. Separations 2023, 10 (1), 57. https://doi.org/10.3390/separations10010057.
28. Aminu, I.; Gumel, S. M.; Ahmad, W. A.; Idris, A. A. Adsorption isotherms and kinetic studies of Congo-Red removal from waste water using activated carbon prepared from jujube seed. Am. J. Anal. Chem. 2020, 11 (1), 47–59. https://doi.org/10.4236/ajac.2020.111004.
29. Javed, T.; Thumma, A.; Uddin, A. N.; Akhter, R.; Taj, M. B.; Zafar, S.; Baig, M. M.; Shah, S. S. A.; Wasim, M.; Abid, M. A.; Masood, T.; Jilani, M. I.; Batool, M. Batch adsorption study of Congo Red dye using unmodified Azadirachta indica leaves: Isotherms and kinetics. Water Pract. Technol. 2024, 19 (2), 546–566. https://doi.org/10.2166/wpt.2024.020.
30. Ali, I. H. Removal of congo red dye from aqueous solution using eco-friendly adsorbent of nanosilica. Baghdad Sci. J. 2021, 18 (2), 0366. https://doi.org/10.21123/bsj.2021.18.2.0366.
31. Ga, A. B. Hydroxyapatite-based materials for heavy metal removal in wastewater treatment. Pet. Petrochem. Eng. J. 2020, 4 (2), 1–5. https://doi.org/10.23880/ppej-16000227.
32. Hughes, J. M.; Rakovan, J. F. Structurally robust, chemically diverse: Apatite and apatite supergroup minerals. Elements 2015, 11 (3), 165–170. https://doi.org/10.2113/gselements.11.3.165.
33. Tas, A. C. Synthesis of biomimetic Ca-hydroxyapatite powders at 37 °C in synthetic body fluids. Biomaterials 2000, 21, 1429–1438.
34. Pokhrel, S. Hydroxyapatite: Preparation, properties and its biomedical applications. Adv. Chem. Eng. Sci. 2018, 8 (4), 225–240. https://doi.org/10.4236/aces.2018.84016.
35. Bose, S.; Ke, D.; Sahasrabudhe, H.; Bandyopadhyay, A. Additive manufacturing of biomaterials. Prog. Mater. Sci. 2017, 93, 45–111. https://doi.org/10.1016/j.pmatsci.2017.08.003.
36. Avram, A.; Frentiu, T.; Horovitz, O.; Mocanu, A.; Goga, F.; Tomoaia-Cotişel, M. Hydroxyapatite for removal of heavy metals from wastewater. Studia Univ. Babeș-Bolyai Chem. 2017, 62 (4), 93–104. https://doi.org/10.24193/subbchem.2017.4.08.
37. Zhou, C.; Wang, X.; Wang, Y.; Song, X.; Fang, D.; Ge, S. The sorption of single- and multi-heavy metals in aqueous solution using enhanced nano-hydroxyapatite assisted with ultrasonic. J. Environ. Chem. Eng. 2021, 9 (3), 105240. https://doi.org/10.1016/j.jece.2021.105240.
38. Billah, R. E. K.; Ayouch, I.; Abdellaoui, Y.; Kassab, Z.; Khan, M. A.; Agunaou, M.; Soufiane, A.; Otero, M.; Jeon, B. A novel chitosan/nano-hydroxyapatite composite for the adsorptive removal of Cd(II) from aqueous solution. Polymers 2023, 15 (6), 1524. https://doi.org/10.3390/polym15061524.

39. Ragab, A.; Ahmed, I.; Bader, D. The removal of Brilliant Green dye from aqueous solution using nano hydroxyapatite/chitosan composite as a sorbent. Molecules 2019, 24 (5), 847. https://doi.org/10.3390/molecules24050847.
40. Hou, H.; Zhou, R.; Wu, P.; Wu, L. Removal of Congo red dye from aqueous solution with hydroxyapatite/chitosan composite. Chem. Eng. J. 2012, 211–212, 336–342. https://doi.org/10.1016/j.cej.2012.09.100.
41. Chahkandi, M. Mechanism of Congo red adsorption on new sol-gel-derived hydroxyapatite nanoparticle. Mater. Chem. Phys. 2017, 202, 340–351. https://doi.org/10.1016/j.matchemphys.2017.09.047.
42. Lee, W.; Loo, C.; Van, K.; Zavgorodniy, A.; Rohanizadeh, R. Regulating protein adsorption onto hydroxyapatite: Amino acid treatment. Key Eng. Mater. 2011, 493–494, 666–671. https://doi.org/10.4028/www.scientific.net/kem.493-494.666.
43. Lee, W.; Loo, C.; Zavgorodniy, A. V.; Rohanizadeh, R. High protein adsorptive capacity of amino acid-functionalized hydroxyapatite. J. Biomed. Mater. Res. A 2012, 101A (3), 873–883. https://doi.org/10.1002/jbm.a.34383.
44. Bumajdad, A.; Hasila, P. Surface modification of date palm activated carbonaceous materials for heavy metal removal and CO2 adsorption. Arab. J. Chem. 2022, 16 (1), 104403. https://doi.org/10.1016/j.arabjc.2022.104403.
45. Uskoković, V.; Uskoković, D. P. Nanosized hydroxyapatite and other calcium phosphates: Chemistry of formation and application as drug and gene delivery agents. J. Biomed. Mater. Res. B 2010, 96B (1), 152–191. https://doi.org/10.1002/jbm.b.31746.
46. El Boujaady, H.; Mourabet, M.; EL Rhilassi, A.; Bennani-Ziatni, M.; El Hamri, R.; Taitai, A. Adsorption of a textile dye on synthesized calcium deficient hydroxyapatite (CDHAp): Kinetic and thermodynamic studies. J. Mater. Environ. Sci. 2016, 7 (11), 4049–4063.
47. Chen, F.; Wang, Z.-C.; Lin, C.-J. Preparation and characterization of nano-sized hydroxyapatite particles and hydroxyapatite/chitosan nanocomposite for use in biomedical materials. Mater. Lett. 2002, 57, 858–861.
48. Lowry, N.; Han, Y.; Meenan, B.; Boyd, A. Strontium and zinc co-substituted nanophase hydroxyapatite. Ceram. Int. 2017, 43 (15), 12070–12078. https://doi.org/10.1016/j.ceramint.2017.06.062.
49. Galotta, A.; Rubenis, K.; Locs, J.; Sglavo, V. M. Dissolution-precipitation synthesis and cold sintering of mussel shells-derived hydroxyapatite and hydroxyapatite/chitosan composites for bone tissue engineering. Open Ceram. 2023, 15, 100418. https://doi.org/10.1016/j.oceram.2023.100418.
50. Kuriakose, T.; Kalkura, S.; Palanichamy, M.; Arivuoli, D.; Dierks, K.; Bocelli, G.; Betzel, C. Synthesis of stoichiometric nanocrystalline hydroxyapatite by ethanol-based sol–gel technique at low temperature. J. Cryst. Growth 2004, 263 (1–4), 517–523. https://doi.org/10.1016/j.jcrysgro.2003.11.057.
51. Panda, R. N.; Hsieh, M. F.; Chung, R. J.; Chin, T. S. FTIR, XRD, SEM and solid state NMR investigations of carbonate-containing hydroxyapatite nanoparticles synthesized by hydroxide-gel technique. J. Phys. Chem. Solids 2003, 64, 193–199.
52. Ma, M. Hierarchically nanostructured hydroxyapatite: Hydrothermal synthesis, morphology control, growth mechanism, and biological activity. Int. J. Nanomedicine 2012, 1781. http://dx.doi.org/10.2147/IJN.S29884.
53. Dreghici, D. B.; Butoi, B.; Predoi, D.; Iconaru, S. L.; Stoican, O.; Groza, A. Chitosan–hydroxyapatite composite layers generated in radio frequency magnetron sputtering discharge: From plasma to structural and morphological analysis of layers. Polymers 2020, 12 (12), 3065. https://doi.org/10.3390/polym12123065.
54. Drabczyk, A.; Kudłacik-Kramarczyk, S.; Głąb, M.; Kędzierska, M.; Jaromin, A.; Mierzwiński, D.; Tyliszczak, B. Physicochemical investigations of chitosan-based hydrogels containing aloe vera designed for biomedical use. Materials 2020, 13 (14), 3073. https://doi.org/10.3390/ma13143073.
55. Gadda, N.; Benabdallah, G. A.; et al. Investigation of equilibrium and kinetics in the removal of Methylene Blue from aqueous solutions using Chamaerops humilis fruit. Morocc. J. Chem. 2024, 12 (4), 1446–1461. https://doi.org/10.48317/IMIST.PRSM/morjchem-v12i4.46755.
56. Chen, Q.; He, Q.; Lv, M.; Xu, Y.; Yang, H.; Liu, X.; Wei, F. Selective adsorption of cationic dyes by UiO-66-NH2. Appl. Surf. Sci. 2014, 327, 77–85. https://doi.org/10.1016/j.apsusc.2014.11.103.
57. Bhattacharyya, K. G.; Gupta, S. S. Adsorptive accumulation of Cd(II), Co(II), Cu(II), Pb(II), and Ni(II) from water on montmorillonite: Influence of acid activation. J. Colloid Interface Sci. 2007, 310 (2), 411–424. https://doi.org/10.1016/j.jcis.2007.01.080.
58. Mohammad, A. M.; Eldin, T. A. S.; Hassan, M. A.; El-Anadouli, B. E. Efficient treatment of lead-containing wastewater by hydroxyapatite/chitosan nanostructures. Arab. J. Chem. 2015, 10 (5), 683–690. https://doi.org/10.1016/j.arabjc.2014.12.016.
59. Adeogun, A. I.; Babu, R. B. One-step synthesized calcium phosphate-based material for the removal of alizarin S dye from aqueous solutions: Isothermal, kinetics, and thermodynamics studies. Appl. Nanosci. 2015, 11 (7), 1–13. https://doi.org/10.1007/s13204-015-0484-9.
60. Mall, I.; Srivastava, V.; Kumar, G.; Mishra, I. Characterization and utilization of mesoporous fertilizer plant waste carbon for adsorptive removal of dyes from aqueous solution. Colloids Surf. A 2006, 278 (1–3), 175–187. https://doi.org/10.1016/j.colsurfa.2005.12.017.
61. Sakkayawong, N.; Thiravetyan, P.; Nakbanpote, W. Adsorption mechanism of synthetic reactive dye wastewater by chitosan. J. Colloid Interface Sci. 2005, 286 (1), 36–42. https://doi.org/10.1016/j.jcis.2005.01.020.

62. Kaur, S.; Rani, S.; Mahajan, R. K. Adsorption kinetics for the removal of hazardous dye congo red by biowaste materials as adsorbents. J. Chem. 2013, 628582. https://doi.org/10.1155/2013/628582.
63. Chiou, M.; Li, H. Equilibrium and kinetic modeling of adsorption of reactive dye on cross-linked chitosan beads. J. Hazard. Mater. 2002, 93 (2), 233–248. https://doi.org/10.1016/S0304-3894(02)00030-4.
64. Wong, S.; Tumari, H. H.; Ngadi, N.; Mohamed, N. B.; Hassan, O.; Mat, R.; Amin, N. A. S. Adsorption of anionic dyes on spent tea leaves modified with polyethyleneimine (PEI-STL). J. Clean. Prod. 2018, 206, 394–406. https://doi.org/10.1016/j.jclepro.2018.09.201.
65. Duranoğlu, D.; Trochimczuk, A. W.; Beker, U. Kinetics and thermodynamics of hexavalent chromium adsorption onto activated carbon derived from acrylonitrile-divinylbenzene copolymer. Chem. Eng. J. 2012, 187, 193–202. https://doi.org/10.1016/j.cej.2012.01.120.
66. Mahmoodi, N. M.; Sadeghi, U.; Maleki, A.; Hayati, B.; Najafi, F. Synthesis of cationic polymeric adsorbent and dye removal isotherm, kinetic and thermodynamic. J. Ind. Eng. Chem. 2013, 20 (5), 2745–2753. https://doi.org/10.1016/j.jiec.2013.11.002.
67. Gerçel, Ö.; Özcan, A.; Özcan, A. S.; Gerçel, H. F. Preparation of activated carbon from a renewable bio-plant of Euphorbia rigida by H2SO4 activation and its adsorption behavior in aqueous solutions. Appl. Surf. Sci. 2006, 253 (11), 4843–4852. https://doi.org/10.1016/j.apsusc.2006.10.053.
68. Al-Harby, N. F.; Albahly, E. F.; Mohamed, N. A. Kinetics, isotherm and thermodynamic studies for efficient adsorption of Congo Red dye from aqueous solution onto novel cyanoguanidine-modified chitosan adsorbent. Polymers 2021, 13 (24), 4446. https://doi.org/10.3390/polym13244446.
69. Mondal, N. K.; Samanta, A.; Chakraborty, S.; Shaikh, W. A. Enhanced chromium(VI) removal using banana peel dust: Isotherms, kinetics and thermodynamics study. Sustain. Water Resour. Manag. 2017, 4 (3), 489–497. https://doi.org/10.1007/s40899-017-0130-7.
70. El-Sharkawy, R.; El-Ghamry, H. A. Multi-walled carbon nanotubes decorated with Cu(II) triazole Schiff base complex for adsorptive removal of synthetic dyes. J. Mol. Liq. 2019, 282, 515–526. https://doi.org/10.1016/j.molliq.2019.02.137.
71. Vijayakumar, G.; Tamilarasan, R.; Dharmendirakumar, M. Adsorption, kinetic, equilibrium and thermodynamic studies on the removal of basic dye Rhodamine-B from aqueous solution by the use of natural adsorbent perlite. J. Mater. Environ. Sci. 2012, 3 (1), 157–170.
72. Mkelemi, M.; Mwaijengo, G. N.; Rwiza, M. "Tree of life": How baobab seeds-derived biochar could lead to water safety for underprivileged communities through heavy metal (Fe) removal – SDG 6. Environ. Sci. Adv. 2024. https://doi.org/10.1039/d4va00205a.
73. Sobhi, H. R.; Yeganeh, M.; Ghambarian, M.; Fallah, S.; Esrafili, A. A new MOF-based modified adsorbent for the efficient removal of Hg(II) ions from aqueous media: Isotherms and kinetics. RSC Adv. 2024, 14 (24), 16617–16623. https://doi.org/10.1039/d4ra00770k.
74. Wu, X.; Hui, K.; Hui, K.; Lee, S.; Zhou, W.; Chen, R.; Hwang, D.; Cho, Y.; Son, Y. Adsorption of basic yellow 87 from aqueous solution onto two different mesoporous adsorbents. Chem. Eng. J. 2011, 180, 91–98. https://doi.org/10.1016/j.cej.2011.11.009.
75. Massad, Y.; Hanbali, G.; Jodeh, S.; Hamed, O.; Bzour, M.; Dagdag, O.; Samhan, S. The efficiency of removal of organophosphorus malathion pesticide using functionalized multi-walled carbon nanotube: Impact of dissolved organic matter (DOM). Sep. Sci. Technol. 2021, 57 (1), 1–12. https://doi.org/10.1080/01496395.2021.1881118.
76. Hanbali, G.; Jodeh, S.; Hamed, O.; Bol, R.; Khalaf, B.; Qdemat, A.; Samhan, S. Enhanced ibuprofen adsorption and desorption on synthesized functionalized magnetic multiwall carbon nanotubes from aqueous solution. Materials 2020, 13 (15), 3329. https://doi.org/10.3390/ma13153329.